using the BOLPs-RGp. The position and intensity of activity were measured during the 200 s immediately after proton irradiation using the trigger signal of the beam-off time. The measurement was performed using the shortest possible distance between the two opposing detector heads of the BOLPs-RGp for each patient. The average distance of the detector heads was 40 cm for the head and neck and the brain, 70 cm for the liver and the lungs, and 50 cm for the prostate. The time of 200 s after proton beam irradiation was chosen according to the intensity of activity estimated from the results of other studies (10, 13). The activity data obtained during proton irradiation were not used for PET imaging. Various types of background radiation (X-rays, gamma rays, and neutrons) occur during proton beam irradiation, and the quality of the activity image becomes markedly worse in their presence (2, 10, 15, 16). Furthermore, high radiation decreases the accuracy of the detector.

Verification of activity measurement was performed in 18, 4, 15, 10, and 1 cases involving tumors of the head and neck, the liver, the lungs, the prostate, and the brain, respectively. The typical fractional dose is 2.5 Gy equivalents (GyE = Gy × the relative biologic effectiveness: [= 1.1 = constant]) for the head and neck, 3.8 GyE for the liver, 4.0 GyE for the lungs, 2.0 GyE for the prostate, and 2.5 GyE for the brain in our facility. The irradiated field is typically planned with three fields in the head and neck and two fields in other sites. Furthermore, the typical number of irradiated field per fractional dose is one in the head and neck, liver, and prostate, and two in the lungs. The fractional dose was delivered over an irradiation time of 10–300 s. The proton beam irradiation was synchronized with the organ motion caused by respiration in the liver and the lungs.

Procedure for clinical use of activity image

A flow chart of procedure for clinical use of the BOLPs-RGp is shown in Fig. 2. In the clinical use, the main operation is to take an activity image every day and compare the activity image of the first day of treatment with each activity image during the comparatively long period of the treatment. If the difference of both the images is confirmed by reducing of the tumor size and changing of the body shape, then the new dose distribution is obtained from redose calculation of the plan on a new CT image acquisition, and the first proton treatment plan is immediately corrected to the new plan. As a result, proton treatments of high accuracy can be offered to the patient by keeping of the planned dose delivery.

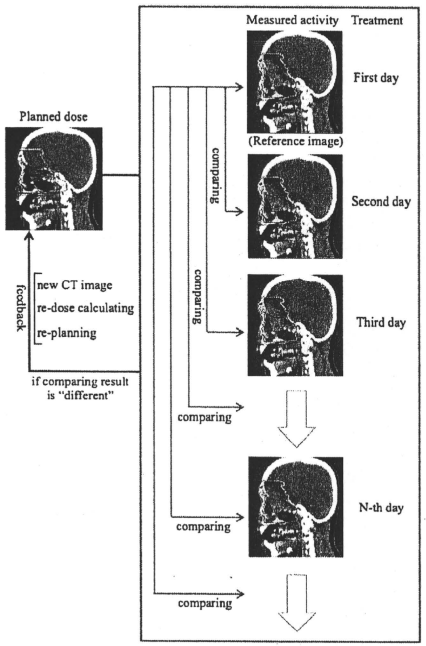

Fig. 2. Flow diagram of the procedure for the clinical use of the BOLPs-RGp.

RESULTS

Estimation of the measurement time for PET imaging

An estimation of an appropriate measurement time for PET imaging was performed using the measured activity data from tumors of the head and neck. The proton beam conditions were as follows: an energy of 120 MeV, a spread out of Bragg peak (SOBP) of 80-mm width, a gantry angle of 340°, a fractional dose of 2.5 GyE, and an irradiation time of 24 s. The distance between the detector heads was 70 cm, and the detection rate of the activity was 1.5 kcps. The left panel of Fig. 3 shows the number of detection events per volume during the detection period after proton beam irradiation. The statistical error (= standard deviation/mean value) decreased as the detection time increased. The error was 2.8% for a 200-s detection time, 3.0% for 150 s, 3.4% for 100 s, and 4.4% for 50 s. The right panel of Fig. 3 shows PET images taken using detection times of (a) 0, (b) 50, (c) 100, and (d) 200 s.

PET images of each treatment site

Typical PET images obtained by the BOLPs-RGp are shown for each case involving tumors of the head and neck, the liver, the lungs, the prostate, and the brain. Figure 4 shows the calculated dose distribution and the measured activity distribution on the first treatment day. The beam irradiation parameters were shown in Table 1. The PET images were obtained during the 200 s after proton beam irradiation. The mean detection rates of the activity generated in the proton beam irradiated volume were 1.58, 1.39, 0.53, 1.08, and 1.85 kcps, respectively. The color line and wash normalized to the iso-center show the dose distribution and activity distribution, respectively. By comparing and verifying between the calculated dose distribution and the measured activity distribution, it can be confirmed visually and roughly that the proton beam has irradiated the tumor. In cases of the liver and the lungs, the length of beam irradiation time is adjusted according to the stability of respiration on the treatment day and the patient. By the effect of organ motion, the number of

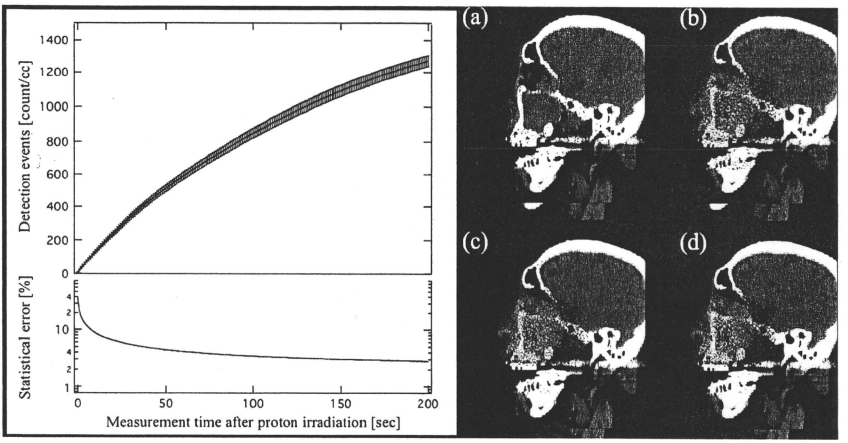

Fig. 3. The number of detection events per volume and PET images obtained during the detection period after proton beam irradiation. The PET images for detection period of (a) 0, (b) 50, (c) 100, and (d) 200 s are shown.

the detection event of the activity measured in the gating window will became about one third of the total detection events, and the statistical error will increase. Therefore, the measurement was performed with no synchronization with organ motion by respiration.

Changes in the activity distribution during the treatment period

In each treatment site, the activity distribution changed probably by reduction of the tumor size and changing of the body shape was conspicuously observed in some cases of the head and neck.

The verification was performed for a case involving tumors of the head and neck. Proton beam irradiation was performed in three fields of view: Port 1: 123 MeV, 90-mm SOBP, 350° gantry angle, 0° bed angle; Port 2: 121 MeV, 90-mm SOBP, 10° gantry angle, 20° bed angle; and Port 3: 117 MeV, 80-mm SOBP, 340° gantry angle, 350° bed angle. The irradiation dose was 2.5 GyE. Figure 5 shows a calculated proton dose distribution, an activity distribution, and a depth profile of a 2.5-GyE dose irradiation after a delivery dose of 2.5 (reference image), 10.0, 17.5, or 32.5 GyE from Port 1, a delivery dose of 5.0 (reference image), 12.5, 20.0, or 35.0 GyE, from Port 2, and a delivery dose of 7.5 (reference image), 15.0, 22.5, or 30.0 GyE from Port 3. Changes of the activity distribution were observed according to changes of the proton beam range and the dose delivered by previous irradiations resulted in a reduction of the tumor (see the arrow and the area surrounded by the dotted line in Fig. 5). The changing values of the activity range for each irradiation field (Port 1, Port 2, and Port 3) are shown in upper left of Fig. 6. The activity range was defined by the depth point of 50% distal falloff in the activity distribution normalized at the iso-center. The changing value of the activity range fully exceeded a 10-mm length. Moreover, to observe the changes in the activity distribution in the depth direction in a similar manner, the ratio of the integration of the detected numbers between 20 mm and 70 mm from the iso-center was expressed as follows:

$$R(D) = \frac{\int_{20}^{70} \left(dA(D)/dZ\right) dz}{\int_{20}^{70} \left(dA(0)/dZ\right) dz}. \quad (1)$$

Here, z is the depth, D is the delivery dose, A(D) is the depth activity distribution, and A(0) is the reference depth activity distribution. The ratio of the delivery dose is shown in the middle left of Fig. 6. The bottom left of Fig. 6 is the proton beam irradiation time per fraction dose at each irradiation. The average of the irradiation time was 30 s, and the difference of the irradiation time at random was within 3 s.

In this case, a new CT image was scanned and a retreatment planning was produced after the delivery of 35 GyE of the prescribed dose of 65 GyE. The volume of the tumor was decreased from 184 mL to 125 mL (the arrow in right of Fig. 6 shows the visible tumor reduction), and the maximum beam range was shortened by 20-mm water equivalent length. In the other 2 cases of 18 clinical cases of the head and neck, the changing activity range of more than 10 mm was observed. Similarly, the new CT image acquisition and the retreatment planning were immediately performed after the observation of the changing activity range. The reduction

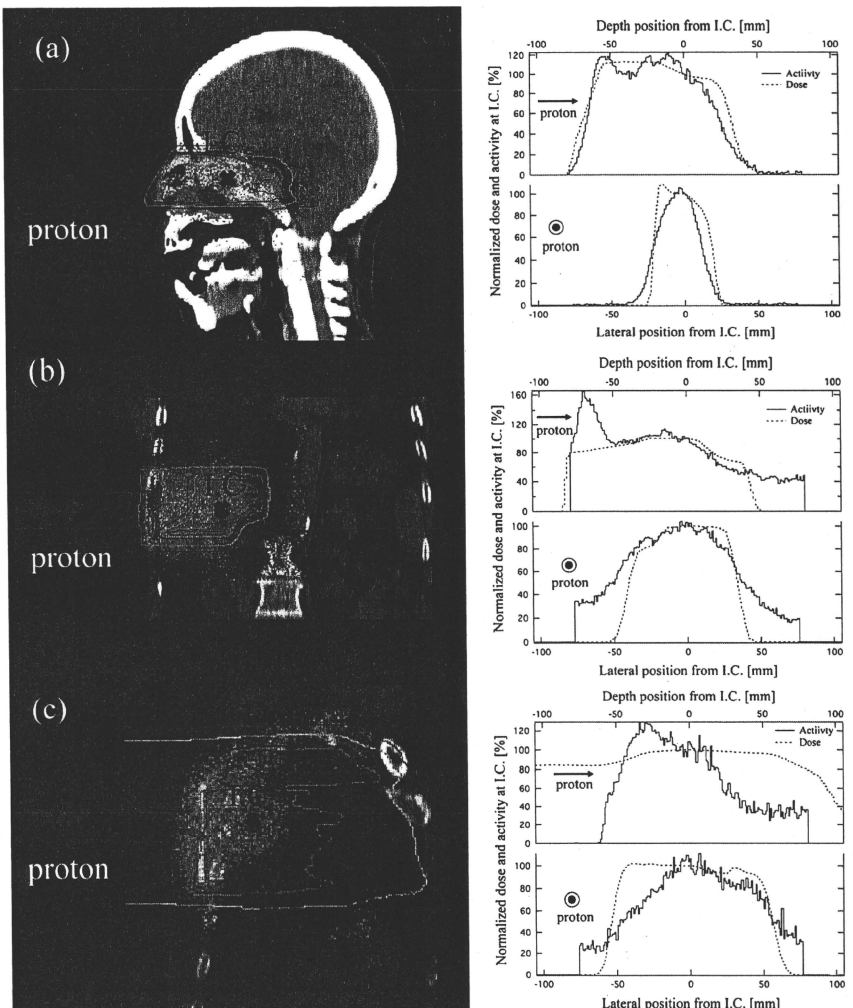

Fig. 4. The calculated dose distribution and the measured activity distribution (left figure), and corresponding lateral and depth profiles (right figure) of the irradiation fields (see Table 1) in each case involving tumors of the head and neck (a), the liver (b), the lungs (c), the prostate (d), and the brain (e), respectively. The iso-dose line of 100% is red, 80% yellowish green, 50% light blue, and 20% purple. The iso-activity wash between 30% and 100% changed from light blue to red.

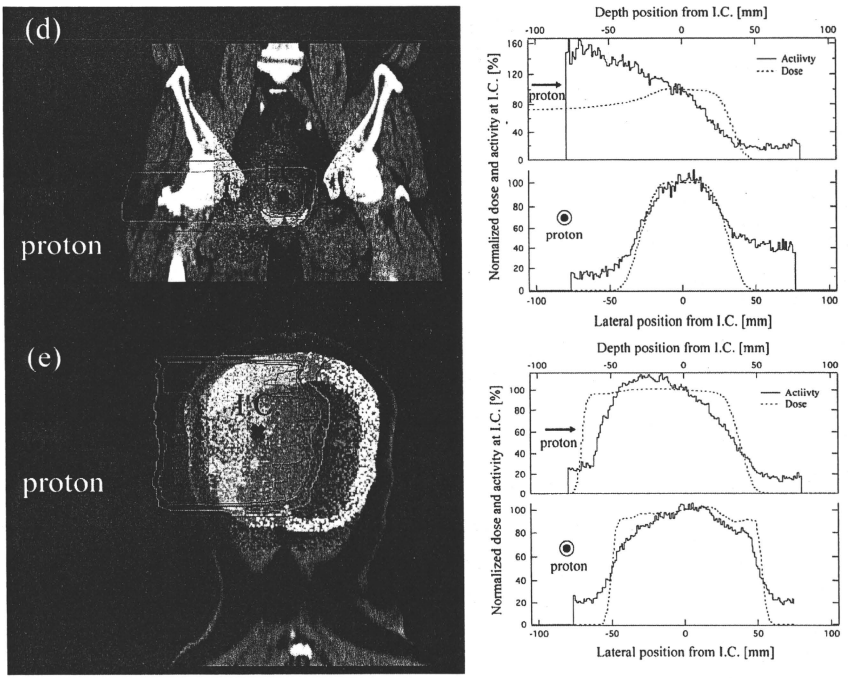

Fig. 4. (*continued*).

of the tumor's volume was more than 100 mL. Also, in carbon therapy, similar observation of the tumor shrinkage has been reported in (7). The BOLPs-RGp indicated that the proton irradiation dose was delivered to the brain stem of organs at risk.

Washout effect of the activity in the treatment period

A histopathologic examination demonstrated that higher activity was observed in regions containing necrotic liver cells than in any other region. The upper panel of Fig. 7 shows the calculated dose distribution and the measured activity distribution on a CT image taken at the first treatment of a 3.8 GyE delivery dose. The bottom left panel of Fig. 7 shows the number of detection counts per 20 s of activity in the regions of interest of areas A and B in the liver. Hence, the region of interest of area A is the necrotic region of the tumor, and area B is the normal tumor region. Therefore, area B-A is equivalent to the area of the tumor minus the necrotic region. The observed decay curves in the region of interest of area A and B-A were fitted well enough using a double exponential equation. The two half-lives of the double exponential fitting were 31 ± 8 s and 146 ± 20 s in the area A, and 21 ± 4 s and 164 ± 11 s in the area B-A, respectively. The half-life was longest in the necrotic region of the tumor. The activity images for the 200 s measurement by the BOLPs-RGp are shown in the left of Fig. 8. The high activity

Table 1. Summary of proton beam irradiation parameters

	Treatment site	Proton energy [MeV]	SOBP [mm]	Gantry angle [deg.]	Bed angle [deg.]	Fractional dose [GyE]	Irradiation time [sec.]
(a)	Head and Neck	123	90	0	0	2.5	39
(b)	Liver	137	70	270	0	3.8	229
(c)	Lungs	145	70	160	0	2.0	38
(d)	Prostate	187	50	270	0	2.0	15
(e)	Brain	122	90	330	90	2.5	40

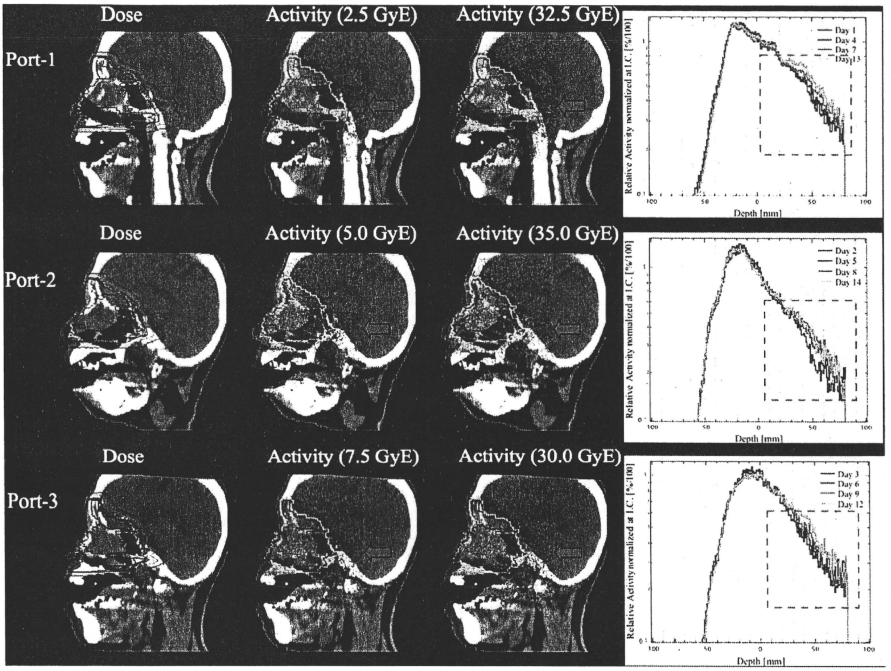

Fig. 5. The calculated proton dose distribution, measured activity distribution of a 2.5-GyE dose irradiation, and the depth profile of the measured activity normalized to the iso-center (0-mm depth) of the reference activity after a delivery dose of 2.5–35.0 GyE.

of the necrotic region decreased to same level as the normal parts of the liver in the last treatment. The ratio F of the detection activity normalized to the activity data from the first treatment for the delivery doses in the area A and the area B-A is expressed as follows:

$$F(D) = \frac{\int_0^{S_A} \left(dN(D)/dS\right) dS / \int_0^{S_A} dS}{\int_{S_A}^{S_B} \left(dN(D)/dS\right) dS / \int_{S_A}^{S_B} dS}. \qquad (2)$$

Here, N is the detection number, S_A is the square of area A, and S_B is the square of area B. Ratio of the F values normalized at the value in first treatment calculated by using Eq. 2 and proton beam irradiation time per fraction dose are shown in the right of Fig. 8. The average of the irradiation time at random was 159 ± 77 s. There was no correction in the irradiation time and the decrease of the activity shown in Fig. 8. A decrease in the activity of the necrotic region was observed after the delivery dose was increased without depending on the beam irradiation time per fraction dose.

DISCUSSION

This study focused on the development of the BOLPs-RGp and its clinical use against tumors of the head and neck, liver, lungs, prostate, and brain in the proton therapy. Quick measurement of the activity generated in a patient's body after proton irradiation is feasible by using the BOLPs-RGp. The elements tracked by the activity imaging are ^{11}C (20.39 min), ^{10}C (19.26 s), ^{13}N (9.965 min), ^{15}O (122.2 s), ^{14}O (70.61 s), ^{30}P (2.498 min), and ^{38}K (7.636 min), and according to the results of a simulation by Parodi *et al.*, the "key" positron emitter nuclei are ^{11}C and ^{15}O (14). The measurement of this activity must be immediately performed after proton irradiation as the half-life of ^{15}O is about 2 min. As a result, the information for activity imaging is obtained in a short period. On the other hand, in the case of a beam OFF-LINE PET system used with a commercial based PET or PET/CT apparatus, it is very difficult to measure the activity of ^{15}O for several minutes even at the start of the activity measurement after proton irradiation. The main elements used for activity imaging are ^{15}O for measurements with

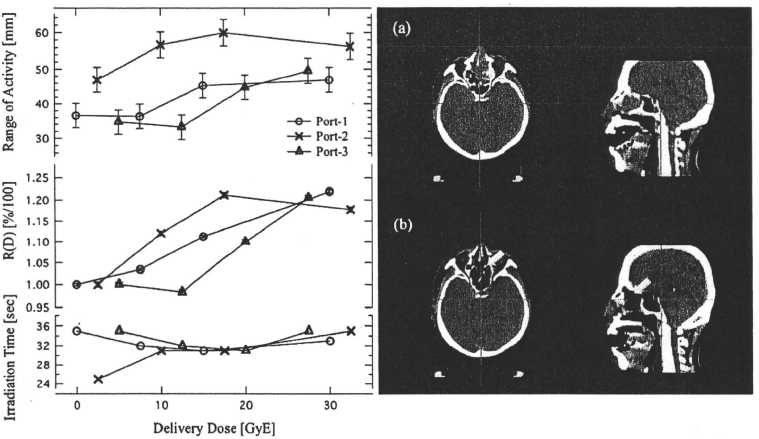

Fig. 6. Changes in the values of the activity range and proton beam irradiation time per fraction dose at each irradiation field of Port-1, Port-2, and Port-3. Axial and sagittal CT images of the head and neck before treatment (a) and after delivery doses of 35 GyE (b).

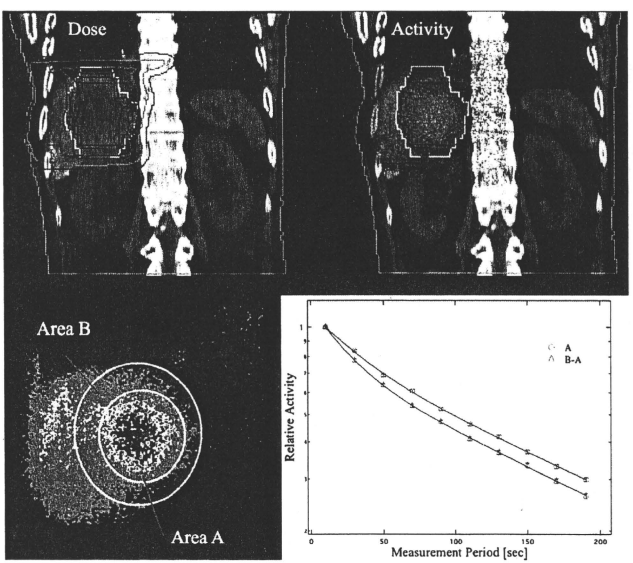

Fig. 7. The calculated dose distribution and the measured activity distribution on a CT image after the first treatment with a 3.8-GyE delivery dose, and the number of detection counts per 20 seconds of the activity in the region of interest (ROI) of areas A and B in the liver.

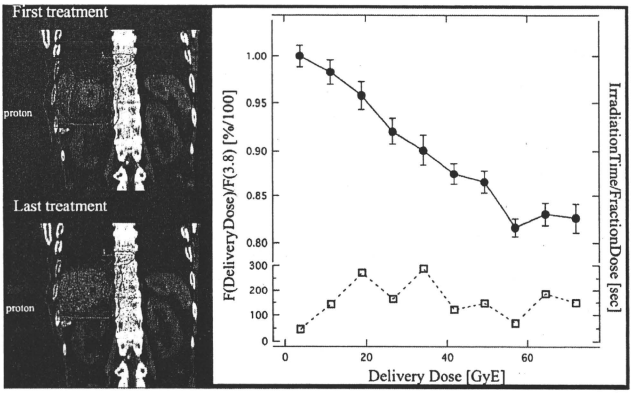

Fig. 8. The activity image and the ratio of the detection number to the measured activity calculated according to Equation (2) in the necrotic region of the liver tumor, and proton beam irradiation time per fractional dose.

the BOLPs-RGp and ^{11}C for measurements with the beam OFF-LINE PET system. As a tumor is equivalent to soft tissue, the measurement of the many ^{15}O nuclei generated in a tumor by proton irradiation is very important for the observation and evaluation of the changing form and the delivery dose response of the tumor. ^{12}C is present and ^{11}C is generated in the adipose tissue. Therefore, high activity is indicated in the region under the skin when using the beam OFF-LINE PET system. Furthermore, the BOLPs-RGp has the advantage of taking measurements with the patient in same position during proton irradiation. However, the CT image for the patient positioning can not be acquired at the same time as the activity measurement when using the BOLPs-RGp. This problem can be solved by the technological introduction of a CBCT.

At present, the length of activity measurement with the BOLPs-RGp after proton beam irradiation is 200 s; but, it may be possible that the measurement time can be shortened to less than 200 s as a result of this research. However, the measurement time must be determined with consideration to the detection efficiency by the delivery dose of each treatment site, the distance between the detector heads, and the activity measurement synchronized with the organ motion caused by respiration in the case of the liver and lungs.

The BOLPs-RGp has been used in the daily proton treatment of 48 patients. The monitoring of the accuracy of the proton beam irradiation was performed by comparing and verifying the daily activity images with reference activity images obtained at the start of the proton treatment. Specially, optimized proton treatment was performed by quickly replanning treatment in three clinical cases involving head-and-neck tumors, because different activity distribution were observed in the two images during the treatment period. The decrease of the activity in the region of necrotic cells in the liver tumor found during the histopathological examination was linked to an increase in the delivery dose. It is suggested that the increase in the washout effect in the necrotic region is caused by a decrease in the number of necrotic cells in the liver because of increased blood flow caused by the higher proton delivery dose. This effect may indicate a need to adapt the treatment to the dose response of the tumors in individual patients as well as the observation of the functional metabolism of organs.

The quality of the activity image is reduced by the large organ motion of the liver and the lungs. In cases of the prostate, the verification of changes in the activity distribution against the condition of the bladder and the position of the head of the femur will be reported in future. Moreover, a study concerning the experimental determination of cross sections of the target nuclear fragment reaction has been completed, and a simulation system that includes our cross-section data for calculating activity distribution in a patient's body with a high accuracy has been constructed using a cluster computer system. Many results of the research of the simulation have been already reported by the study group of Parodi *et al.* (12, 14). Finally, the ideal DGPT will be achieved through these developments and the research.

CONCLUSIONS

A BOLPs-RGp was constructed in our proton treatment room. The BOLPs-RGp has been used in many clinical cases. Report of the clinical use with beam ON-LINE PET or in-beam PET in the proton therapy has been never done before. The daily activity images obtained indicated the proton irradiation volume of the treatment administered to patients. Information about the positron-emitting nuclei provided by the BOLPs-RGp will be important for improving proton treatment accuracy in the future. DGPT (10) will thereby be achieved via daily proton treatment using the BOLPs-RGp.

REFERENCES

1. Oelfke U, Lam G, Atkins M. Proton dose monitoring with PET: Quantitative studies in Lucite. *Phys Med Biol* 1996;41: 177–196.
2. Litzenberg DW, Roberts DA, Lee MY, *et al.* On-line monitoring of radiotherapy beams: Experimental results with proton beams. *Med Phys* 1999;26:992–1006.
3. Parodi K, Enghardt W. Potential application of PET in quality assurance of proton therapy. *Phys Med Biol* 2000;45:N151–N156.
4. Nishio T, Ogino T, Shimbo M, *et al.* Distributions of b⁺ decayed nucleus produced from the target fragment reaction in $(CH_2)n$ and patient liver targets by using a proton beam for therapy. *Abstr XXXIV PTCOG Mtg Boston* 2001;15–16.
5. Parodi K, Enghardt W, Haberer T. In-beam PET measurements of β^+ radioactivity induced by proton beams. *Phys Med Biol* 2002;47:21–36.
6. Hishikawa Y, Kagawa K, Murakami M, *et al.* Usefulness of positron-emission tomographic images after proton therapy. *Int J Radiat Oncol Biol Phys* 2002;53:1388–1391.
7. Enghardt W, Parodi K, Crespo P, *et al.* Dose quantification from in-beam positron emission tomography. *Radiother Oncol Suppl* 2 2004;73:S96–S98.
8. Nishio T, Sato T, Kitamura H, *et al.* Distributions of β^+ decayed nuclei generated in the CH_2 and H_2O targets by the target nuclear fragment reaction using therapeutic MONO and SOBP proton beam. *Med Phys* 2005;32:1070–1082.
9. Parodi K, Ponisch F, Enghardt W. Experimental study on the feasibility of in-beam PET for accurate monitoring of proton therapy. *IEEE Trans Nucl Sci* 2005;52:778–786.
10. Nishio T, Ogino T, Nomura K, *et al.* Dose-volume delivery guided proton therapy using beam ON-LINE PET system. *Med Phys* 2006;33:4190–4197.
11. Parodi K, Paganetti H, Cascio E, *et al.* PET/CT imaging for treatment verification after proton therapy: A study with plastic phantoms and metallic implants. *Med Phys* 2007;34: 419–435.
12. Parodi K, Paganetti H, Shih HA, *et al.* Patient study of in vivo verification of beam delivery and range, using positron emission tomography and computed tomography imaging after proton therapy. *Int J Radiat Oncol Biol Phys* 2007;68:920–934.
13. Nishio T, Miyatake A, Inoue K, *et al.* Experimental verification of proton beam monitoring in a human body by use of activity image of positron-emitting nuclei generated by nuclear fragmentation reaction. *Radiol Phys Technol* 2008;1: 44–54.
14. Parodi K, Ferrari A, Sommerer F, *et al.* Clinical CT-based calculations of dose and positron emitter distributions in proton therapy using the FLUKA Monte Carlo code. *Phys Med Biol* 2007;52:3369–3387.
15. Pawelke J, Enghardt W, Haberer T, *et al.* In-beam PET imaging for the control of heavy-ion tumour therapy. *IEEE Trans Nucl Sci* 1997;44:1492–1498.
16. Parodi K, Crespo P, Eickhoff H, *et al.* Random coincidences during in-beam PET measurements at microbunched therapeutic ion beams. *Nucl Instrum Meth A* 2005;545:446–458.
17. Uchida H, Okamoto T, Ohmura T, *et al.* A compact planar positron imaging system. *Nucl Instr Meth* 2004;A516:564–574.

Lung Cancer 69 (2010) 315–318

Contents lists available at ScienceDirect

Lung Cancer

journal homepage: www.elsevier.com/locate/lungcan

Re-challenge chemotherapy for relapsed non-small-cell lung cancer

Tatsuya Nagano[a], Young Hak Kim[b,*], Koichi Goto[a], Kaoru Kubota[a], Hironobu Ohmatsu[a], Seiji Niho[a], Kiyotaka Yoh[a], Yoichi Naito[a], Nagahiro Saijo[a], Yutaka Nishiwaki[a]

[a] Division of Thoracic Oncology, National Cancer Center Hospital East, Kashiwa, Chiba, Japan
[b] Department of Respiratory Medicine, Graduate School of Medicine, Kyoto University, 54 Shogoin-Kawaharacho, Sakyo-ku, Kyoto 606-8507, Japan

ARTICLE INFO

Article history:
Received 22 July 2009
Received in revised form
10 November 2009
Accepted 15 November 2009

Keywords:
Re-challenge chemotherapy
Non-small-cell lung cancer
Second-line chemotherapy
Relapse
Platinum-based
Docetaxel

ABSTRACT

There has been no report about re-challenge chemotherapy (RC) consisting of the same regimen as first-line chemotherapy in non-small-cell lung cancer (NSCLC). The aim of this study was to evaluate the efficacy of RC as second-line chemotherapy in patients with relapsed NSCLC. We conducted a retrospective review of 28 consecutive NSCLC patients who were treated with RC and compared their clinical outcomes with those of 38 consecutive NSCLC patients who were treated with docetaxel (DOC) at our hospital between July 1992 and December 2003. The RC group consisted of 21 men and 7 women, with a median age of 62 years (range, 42–76 years). Most first-line regimens were platinum-based and the median administered course was 3 (range, 2–7). All patients had responded to the first-line chemotherapy and had performance status (PS) 1 at relapse. The median interval from the end of first-line chemotherapy to relapse was 5.0 months (range, 1.6–36.1 months). The overall response rate of RC was 29%. The median survival time from the beginning of RC was 17.0 months and the 1-year survival rate was 60%. RC led to a significantly better overall survival rate than DOC ($p = 0.0342$). RC could be an active second-line regimen in patients with relapsed NSCLC who responded to first-line chemotherapy.

© 2009 Elsevier Ireland Ltd. All rights reserved.

1. Introduction

Lung cancer is one of the most common causes of death from cancer worldwide. Non-small-cell lung cancer (NSCLC) accounts for at least 80% of all lung cancer cases and about 65–80% of NSCLC patients present with locally advanced or metastatic disease [1]. Today, standard first-line chemotherapy for advanced NSCLC patients with a good performance status (PS) is considered to be the platinum-based doublet regimen [2,3]. In a Japanese phase III study comparing four different platinum doublet regimens, response rates of 30–33%, and median survival time (MST) of 11–14 months were reported [2].

The prognosis of patients who have relapsed or have refractory NSCLC after first-line chemotherapy and did not receive additional therapy is abysmal: MST after relapse was reported to be only 3 months [4]. Some cytotoxic agents, such as docetaxel (DOC) [5,6] and pemetrexed [7], or molecular target agents, such as gefitinib [8] and erlotinib [9], are active in the second-line or third-line setting; however, further progress is needed in the treatment of relapsed NSCLC.

In general, relapsed tumors are thought to have acquired resistance to previously administered drugs [10,11]; however, we consider that some relapsed tumors of NSCLC might still be sensitive to the prior chemotherapy, as in sensitive relapse in small-cell lung cancer (SCLC). In this study, we conducted a retrospective review of 28 consecutive NSCLC patients who received re-challenge chemotherapy (RC) as second-line chemotherapy and compared their clinical outcomes with those of 38 consecutive NSCLC patients who were treated with DOC, which has been used as standard second-line chemotherapy in Japan, at our hospital to evaluate the efficacy of RC for relapsed NSCLC.

2. Materials and methods

2.1. Patients

Between July 1992 and December 2003, 3934 consecutive NSCLC patients were treated at the National Cancer Center Hospital East, Japan, including 579 patients who had received second-line chemotherapy. In this study, we conducted a retrospective review of the 28 consecutive patients who underwent RC and the 38 consecutive patients who had responded to first-line therapy and received DOC as the second-line therapy, and compared the clinical outcomes between the two treatment groups. In both the groups, patients received second-line chemotherapy after they experienced disease progression. All patients in the RC group had Eastern Cooperative Oncology Group (ECOG) PS 1; therefore, DOC group patients were restricted to PS ≤1 to balance patient backgrounds.

* Corresponding author. Tel.: +81 75 751 3830; fax: +81 75 751 4643.
E-mail address: ekim@kuhp.kyoto-u.ac.jp (Y.H. Kim).

0169-5002/$ – see front matter © 2009 Elsevier Ireland Ltd. All rights reserved.
doi:10.1016/j.lungcan.2009.11.016

Table 1
Patient characteristics.

Characteristics	RC (n=28)	DOC (n=38)	p value
Age (years)			
Median	62	67	0.388
Range	42–76	47–77	
Gender (%)			
Male	21(75)	33(87)	0.333
Female	7(25)	5(13)	
Smoking status (%)			
Non-smoker	4(14)	4(11)	0.714
Smoker	24(86)	34(89)	
PS (ECOG) (%)			
0	0(0)	4(11)	0.131
1	28(100)	34(89)	
Clinical stage (%)			
IIB	0(0)	2(5)	0.029
IIIA	1(4)	7(18)	
IIIB	14(50)	22(58)	
IV	13(46)	7(18)	
Histology (%)			
Ad	18(64)	16(42)	0.087
Sq	7(25)	17(45)	
Others	3(11)	5(13)	

RC, re-challenge chemotherapy; DOC, docetaxel; PS, performance status; ECOG, Eastern Cooperative Oncology Group; Ad, adenocarcinoma; Sq, squamous cell carcinoma.

2.2. Treatment and response assessment

RC was defined as the same chemotherapy regimen as the first-line chemotherapy. The Response Evaluation Criteria in Solid Tumors (RECIST) [12] was used to evaluate the response of patients and objective tumor response was assessed as complete response (CR), partial response (PR), stable disease (SD), and progressive disease (PD). This response assessment was based on the disease progressive state after first-line therapy in both the groups.

2.3. Statistical analysis

All statistical analyses were performed with SPSS 11.0 statistical software (Dr. SPSS II for Windows, Standard version 11.0; SPSS Inc., Chicago, IL). Differences in patient characteristics between groups were tested for significance using the χ^2 test or Fisher's exact test, as appropriate, and the Mann–Whitney U-test was used to compare the number of courses and intervals. Overall survival (OS) was measured from the start of second-line chemotherapy to the date of death from any cause or the date that patients were last known to be alive. Survival rates were calculated by the Kaplan–Meier method, and the statistical significance of any difference in OS was evaluated by the log-rank test. p values <0.05 were considered significant.

3. Results

3.1. Patient characteristics

Patient characteristics are shown in Table 1. All clinical data were retrieved from medical records. The two treatment groups were well balanced for age, gender, smoking status, and PS, with the exception of histology and clinical stage: the RC group had more advanced stages (p = 0.029) and tended to have more adenocarcinoma than the DOC group (p = 0.087).

The majority of patients were treated with a platinum-based regimen as first-line chemotherapy and only two patients in each group had received non-platinum chemotherapy (Table 2). All patients in both groups had responded (PR/CR) to first-line chemotherapy. The median number of cycles of first-line chemotherapy was 3 in each group and the median interval from the end of first-line chemotherapy to relapse was 5.0 months (range, 1.6–36.1 months) in the RC group and 7.6 months (range, 0.7–41.1 months) in the DOC group (p = 0.165).

Table 2
Details of first-line chemotherapy.

	RC (n=28)	DOC (n=38)	p value
Course			
Median	3	3	0.098
Range	2–7	1–6	
Regimen, cases	10	4	
CDDP+MMC+VDS			
CDDP+VDS	7	2	
CDDP+VNR	3	28	
CDDP+DOC	3	0	
CDDP+GEM	1	0	
CDDP+CPT	1	2	
CBDCA+PTX	1	0	
GEM+VNR	2	1	
VNR	0	1	
Response, cases			
CR	1	1	1.000
PR	27	37	
Interval from the end of first-line chemotherapy to relapse, months			
Median	5.0	7.6	0.165
Range	1.6–36.1	0.7–41.1	

RC, re-challenge chemotherapy; DOC, docetaxel; CDDP, cisplatin; MMC, mitomycin C; VDS, vindesine; VNR, vinorelbine; GEM, gemcitabine; CPT, camptothecin; CBDCA, carboplatin; PTX, paclitaxel; CR, complete response; PR, partial response.

Patients in the RC group received a median of 1.5 cycles (range, 1–3) of RC, whereas 2.0 cycles (range, 1–10) of DOC in the DOC group. One patient in the RC group discontinued RC with cisplatin and docetaxel at 1 cycle because of severe allergy and no patients died of toxicity from RC. The proportion of patients who received third-line and fourth-line chemotherapy was well balanced between the two treatment groups (Table 3).

3.2. Response and survival

Response and survival in each group are shown in Table 4, and the Kaplan–Meier curve for overall survival is shown in Fig. 1. The median follow-up time was 20.4 months. In the RC group, 20 patients died during the follow-up period. One patient died of

Table 3
Additional chemotherapy after re-challenge chemotherapy and docetaxel.

	RC (n=28)	DOC (n=38)
Third-line chemotherapy		
CDDP+VNR	2(8)	0(0)
DOC	3(11)	0(0)
Gefitinib	3(11)	8(21)
Erlotinib	0(0)	1(3)
GEM	0(0)	4(11)
GEM+VNR	1(3)	2(5)
Total (%)	9(32)	15(40)
Fourth-line chemotherapy		
DOC	1(3)	0(0)
Gefitinib	2(8)	1(3)
GEM+VNR	0(0)	1(3)
GEM+DOC	1(3)	0(0)
CBDCA+PTX	0(0)	1(3)
Total (%)	4(14)	3(8)

RC, re-challenge chemotherapy; DOC, docetaxel; CDDP, cisplatin; VNR, vinorelbine; GEM, gemcitabine; CBDCA, carboplatin; PTX, paclitaxel.

Table 4
Treatment efficacy of re-challenge chemotherapy and docetaxel.

	RC (n = 28)	DOC (n = 38)	p value
Response (%)			
Overall response	8 (29)	3 (7.9)	0.043
CR	0	0	
PR	8	3	
SD	13	16	
PD	7	19	
Survival			
Median, months	17.0	9.0	0.0342
Range	0.4–43.0	1.3–31.4	
1-Year survival	60	29	

RC, re-challenge chemotherapy; DOC, docetaxel; CR, complete response; PR, partial response; SD, stable disease; PD, progressive disease.

unknown cause after receiving chemotherapy with cisplatin, mitomycin C, and vindesine (CMV), and 19 patients died of lung cancer. The overall response rate was 29% in the RC group and 8% in the DOC group, respectively (p = 0.043). The median survival time (MST) and 1-year survival rate from the beginning of second-line chemotherapy were 17.0 months and 60% in the RC group, and 9.0 months and 29% in the DOC group, respectively. The OS of the RC group was significantly better than that of the DOC group (p = 0.0342).

4. Discussion

To our knowledge, this is the first report to evaluate the efficacy of RC in relapsed NSCLC patients, demonstrating an excellent response rate and survival.

DOC is a standard second-line chemotherapy regimen, and has been most widely used in Japan. A randomized phase III study comparing DOC with best supportive care showed better OS for DOC patients (7.5 months vs. 4.6 months, p = 0.047) [6]. Another phase III study showed that the 1-year survival rate of patients who received DOC 75 mg/m^2 was significantly better than that of patients who received vinorelbine or ifosfamide (32% vs. 19%; p = 0.025) [5]; however, these studies included patients who had not responded to first-line chemotherapy and patients who had PS 2.

In this study, we also conducted a retrospective review of patients who had received DOC as the second-line chemotherapy under the same conditions, namely, patients with PS 0–1 and complete or partial response to prior therapy in the same period. The MST and 1-year survival rate in the DOC group were 9.0 months and 29%, respectively. These survival data were comparable to those demonstrated in the phase III studies above. By contrast, the RC group showed MST of 17.0 months and a 60% 1-year survival rate. These were significantly better than in the DOC group, although more stage IV patients were included in the RC group. The RC group tended to include more adenocarcinoma patients; however, subsequent treatments were similar between groups and the proportion of patients administered gefitinib was almost the same. These results suggested that RC had a sufficient anti-tumor effect and could be an effective second-line regimen for certain types of relapsed NSCLC.

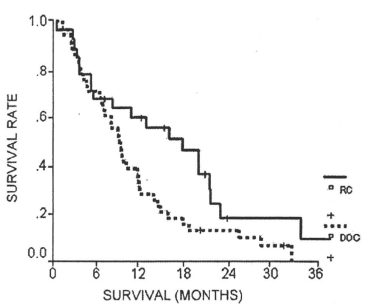

Fig. 1. Kaplan–Meier curve for overall survival. Overall survival in the re-challenge chemotherapy (RC) group was significantly better than in the docetaxel (DOC) group (log-rank test, p = 0.0342).

The interval from first-line to second-line chemotherapy was quite variable in both the groups. Therefore, limiting the patients whose treatment-free interval of more than 6 months, MST was 21.4 months in the RC group (n = 11), and 9.5 months in the DOC group (n = 23), respectively (p = 0.0110).

Drug resistance is considered a major limitation of chemotherapy. Resistance to anticancer drugs is most often ascribed to gene mutations, gene amplification, or epigenetic changes that influence the uptake, metabolism, or export of drugs from a single agent [13]. Although a detailed explanation for re-induction has not been presented, the observation of SCLC cell line resistance during exposure to doxorubicin that disappeared after drug withdrawal provides some suggestions [14]. In a group of SCLC patients, 37 responded to first-line treatment, resulting in 6 CR and 17 PR by RC treatment [15]. In a study by Giaccone et al. of a group of 13 patients with a response duration of 30 weeks or longer, RC at relapse resulted in 6 patients having a second response [16]. These results illustrate that RC was effective in sensitive SCLC patients and encouraged us to evaluate the same phenomenon; that is, some tumors had less drug resistance and were sensitive to their previous anticancer drugs during chemotherapy for NSCLC.

The results should be interpreted with caution because there might be a potential imbalance of prognostic factors between the groups. Nevertheless, this study may suggest that RC has potential to become a treatment option for relapsed NSCLC patients if the previous chemotherapy had been effective and relapsed patients maintained good PS.

Conflict of interest statement

We have no conflict of interest and financial support to declare.

References

[1] Novello S, Le Chevalier T. Chemotherapy for non-small-cell lung cancer. Part 1: early-stage disease. Oncology 2003;17:357–64 [Williston Park].
[2] Ohe Y, Ohashi Y, Kubota K, Tamura T, Nakagawa K, Negoro S, et al. Randomized phase III study of cisplatin plus irinotecan versus carboplatin plus paclitaxel, cisplatin plus gemcitabine, and cisplatin plus vinorelbine for advanced non-small-cell lung cancer: Four-Arm Cooperative Study in Japan. Ann Oncol 2007;18:317–23.
[3] Schiller JH, Harrington D, Belani CP, Langer C, Sandler A, Krook J, et al. Comparison of four chemotherapy regimens for advanced non-small-cell lung cancer. N Engl J Med 2002;346:92–8.
[4] Clinical practice guidelines for the treatment of unresectable non-small-cell lung cancer. Adopted on May 16, 1997 by the American Society of Clinical Oncology. J Clin Oncol 1997;15:2996–3018.
[5] Fossella FV, DeVore R, Kerr RN, Crawford J, Natale RR, Dunphy F, et al. Randomized phase III trial of docetaxel versus vinorelbine or ifosfamide in patients with advanced non-small-cell lung cancer previously treated with platinum-containing chemotherapy regimens. The TAX 320 Non-Small Cell Lung Cancer Study Group. J Clin Oncol 2000;18:2354–62.
[6] Shepherd FA, Dancey J, Ramlau R, Mattson K, Gralla R, O'Rourke M, et al. Prospective randomized trial of docetaxel versus best supportive care in patients with non-small-cell lung cancer previously treated with platinum-based chemotherapy. J Clin Oncol 2000;18:2095–103.
[7] Hanna N, Shepherd FA, Fossella FV, Pereira JR, De Marinis F, von Pawel J, et al. Randomized phase III trial of pemetrexed versus docetaxel in patients with non-small-cell lung cancer previously treated with chemotherapy. J Clin Oncol 2004;22:1589–97.
[8] Kim E, Hirsh V, Mok T, Socinski M, Gervais R, Wu Y, et al. Gefitinib versus docetaxel in previously treated non-small-cell lung cancer (INTEREST): a randomised phase III trial. Lancet 2008;372:1809–18.

[9] Shepherd FA, Rodrigues Pereira J, Ciuleanu T, Tan EH, Hirsh V, Thongprasert S, et al. Erlotinib in previously treated non-small-cell lung cancer. N Engl J Med 2005;353:123–32.
[10] Hochhauser D, Harris AL. Drug resistance. Br Med Bull 1991;47:178–96.
[11] Sawyers CL. Where lies the blame for resistance – tumor or host? Nat Med 2007;13:1144–5.
[12] Therasse P, Arbuck SG, Eisenhauer EA, Wanders J, Kaplan RS, Rubinstein L, et al. New guidelines to evaluate the response to treatment in solid tumors. European Organization for Research and Treatment of Cancer, National Cancer Institute of the United States, National Cancer Institute of Canada. J Natl Cancer Inst 2000;92:205–16.
[13] Tredan O, Galmarini CM, Patel K, Tannock IF. Drug resistance and the solid tumor microenvironment. J Natl Cancer Inst 2007;99:1441–54.
[14] Zijlstra JG, de Vries EG, Mulder NH. Multifactorial drug resistance in an adriamycin-resistant human small cell lung carcinoma cell line. Cancer Res 1987;47:1780–4.
[15] Postmus PE, Berendsen HH, van Zandwijk N, Splinter TA, Burghouts JT, Bakker W. Retreatment with the induction regimen in small cell lung cancer relapsing after an initial response to short term chemotherapy. Eur J Cancer Clin Oncol 1987;23:1409–11.
[16] Giaccone G, Ferrati P, Donadio M, Testore F, Calciati A. Reinduction chemotherapy in small cell lung cancer. Eur J Cancer Clin Oncol 1987;23:1697–9.

original article

Annals of Oncology 21: 255–262, 2010
doi:10.1093/annonc/mdp304
Published online 24 July 2009

Association between gain-of-function mutations in *PIK3CA* and resistance to HER2-targeted agents in *HER2*-amplified breast cancer cell lines

Y. Kataoka[1], T. Mukohara[2,3]*, H. Shimada[4], N. Saijo[4], M. Hirai[1] & H. Minami[2,3]

[1]*Hospital Pharmacy;* [2]*Cancer Center, Kobe University Hospital;* [3]*Medical Oncology, Department of Medicine, Kobe University Graduate School of Medicine, Chuo-ku, Kobe and* [4]*Research Center for Innovative Oncology, National Cancer Hospital East, Kashiwa, Japan*

Received 24 April 2009; accepted 4 May 2009

Background: The mechanism of resistance to human epidermal growth factor receptor 2 (HER2)-targeted agents has not been fully understood. We investigated the influence of *PIK3CA* mutations on sensitivity to HER2-targeted agents in naturally derived breast cancer cells.

Materials and methods: We examined the effects of Calbiochem (CL)-387,785, HER2 tyrosine kinase inhibitor, and trastuzumab on cell growth and *HER2* signaling in eight breast cancer cell lines showing *HER2* amplification and trastuzumab-conditioned BT474 (BT474-TR).

Results: Four cell lines with *PIK3CA* mutations (E545K and H1047R) were more resistant to trastuzumab than the remaining four without mutations (mean percentage of control with 10 μg/ml trastuzumab: 58% versus 92%; $P = 0.010$). While *PIK3CA*-mutant cells were more resistant to CL-387,785 than *PIK3CA*-wild-type cells (mean percentage of control with 1 μM CL-387,785: 21% versus 77%; $P = 0.001$), CL-387,785 retained activity against BT474-TR. Growth inhibition by trastuzumab and CL-387,785 was more closely correlated with changes in phosphorylation of S6K (correlation coefficient, 0.811) than those of HER2, Akt, or ERK1/2. Growth of most *HER2*-amplified cells was inhibited by LY294002, regardless of *PIK3CA* genotype.

Conclusions: *PIK3CA* mutations are associated with resistance to HER2-targeted agents. PI3K inhibitors are potentially effective in overcoming trastuzumab resistance caused by *PIK3CA* mutations. S6K phosphorylation is a possibly useful pharmacodynamic marker in HER2-targeted therapy.

Key words: breast cancer, HER2, *PIK3CA*, trastuzumab

introduction

Breast cancer is the leading cause of cancer death among women worldwide, with ~1 million new cases reported each year [1, 2]. Approximately 20% of breast cancer tumors show overexpression of the HER2 protein, which is mainly caused by gene amplification. HER2 overexpression has been repeatedly identified as a poor prognostic factor [3, 4]. Trastuzumab is a humanized mAb targeting the extracellular domain of the HER2 protein. From the late 1990s, clinical studies have intensively evaluated the therapeutic roles of trastuzumab. For the treatment of HER2-overexpressing metastatic breast cancers, studies report that a combination of trastuzumab and conventional chemotherapy shows significantly higher efficacy than chemotherapy alone [5]. The use of trastuzumab has extended to the treatment of operable HER2-overexpressing breast cancer as an adjuvant or neoadjuvant [6–8]. Despite promising usefulness in clinics, a modest percentage of patients are reported to benefit from trastuzumab therapy, with response rates to trastuzumab as a single agent of ~20% [9]. In addition, even when trastuzumab therapy leads to temporary tumor shrinkage, clinical relapse is observed for the vast majority of metastatic patients. To develop adequate therapies capable of overcoming primary and secondary resistance to trastuzumab, a better understanding of the resistance mechanism is crucial.

To date, several mechanisms of primary resistance to trastuzumab have been proposed. A series of studies indicated that trastuzumab resistance is due to the truncated form of HER2, which lacks an extracellular domain to which trastuzumab is indicated to attach [10, 11]. Nagata et al. [12] demonstrated that loss of phosphatase and tensin homolog deleted on chromosome 10 (PTEN), a negative regulator of PI3K, correlates with poor response to trastuzumab. More recently, the roles of *PIK3CA* in trastuzumab resistance have been under particular investigation. Somatic mutations of *PIK3CA* were first identified in 2004 in various malignant tumors including breast cancer [13]. Subsequent studies have reported that the E545K and H1047R hotspot mutations, found

*Correspondence to: Dr T. Mukohara, Department of Medical Oncology, Kobe University Hospital, 7-5-2, Kusunoki-cho, Chuo-ku, Kobe 650-0017, Japan. Tel: +81-78-382-5825; Fax: +81-78-382-5821; E-mail: mukohara@med.kobe-u.ac.jp

© The Author 2009. Published by Oxford University Press on behalf of the European Society for Medical Oncology.
All rights reserved. For permissions, please email: journals.permissions@oxfordjournals.org

on exons 9 and 20, respectively, are the most frequent types of mutation, found in 8%–40% of breast cancer tumors [13–16]. Both hotspot mutations are gain-of-function mutations which transform normal mammary epithelial cells [17, 18]. Berns et al. [19] investigated the roles of gain-of-function mutations of the *PIK3CA* gene in trastuzumab resistance by transfecting wild-type and mutant (H1047R) forms of *PIK3CA* in SKBR-3 HER2-overexpressing breast cancer cells. Results showed that compared with green fluorescent protein (GFP) control, both wild-type and mutant *PIK3CA* transfections resulted in trastuzumab resistance. Further, analysis of *PIK3CA* genotypes in tumor samples obtained from breast cancer patients having undergone trastuzumab-based therapy showed an association between the presence of *PIK3CA* hotspot mutations and shorter time to progression after therapy [19].

Tyrosine kinase inhibitors (TKIs) have also been investigated as potential agents against trastuzumab resistance [20]. A clinical study in metastatic breast cancer patients having previously experienced tumor progression under trastuzumab-based therapies showed that compared with capecitabine alone, treatment using a combination of capecitabine with lapatinib, a dual inhibitor of epidermal growth factor receptor (EGFR) and HER2 tyrosine kinase, lead to significantly longer time to progression [21]. Eichhorn et al. [22], however, demonstrated that transfection of mutant *PIK3CA* (H1047R) in BT474 HER2-overexpressing breast cancer cells resulted in resistance to lapatinib compared with parental cells. Further, results showed that resistance was overcome using NVP-BEZ235, a PI3K and mammalian target of rapamycin dual inhibitor [22].

These findings based on gene manipulations indicate that gain-of-function mutations in the *PIK3CA* gene lead to resistance to trastuzumab, as well as HER2-TKI. To our knowledge, however, these findings have not been confirmed in naturally derived breast cancer cells. Here, trastuzumab resistance due to *PIK3CA* mutations was evaluated in eight naturally derived breast cancer cell lines harboring *HER2* gene amplification. Further, possible therapeutic means to overcome primary and secondary resistance to trastuzumab were investigated, as well as potential pharmacodynamic markers correlated with the growth-inhibitory effect of HER2-targeted drugs.

materials and methods

cell culture

MCF-7, MDA-MB-361, HCC1954, MDA-MB-453, UACC893, CAMA-1, MDA-MB-435S, MDA-MB-415, ZR75-30, HCC70, MDA-MB-468, and HCC1419 cell lines were purchased from the American Type Culture Collection (Manassas, VA). BT474, SKBR-3, BT549, T47D, ZR75-1, and MDA-MB-231 cells were kindly provided by Ian Krop of the Dana-Farber Cancer Institute. Of the 18 breast cancer cell lines, eight (ZR75-30, BT474, SKBR-3, HCC1419, MDA-MB-453, MDA-MB-361, HCC1954, and UACC 893) were reported to have *HER2* gene amplification [23], with levels of PTEN protein expression equivalent to those reported in our previous study [24]. Among the *HER2*-amplified cell lines, ZR75-30, SKBR-3, and HCC1419 were reported to contain the wild-type *PIK3CA* gene and MDA-MB-453, MDA-MB-361, HCC1954, and UACC893 hotspot *PIK3CA* mutations (Table 1) [14]. BT474 was reported to contain a relatively rare type of *PIK3CA* mutation at exon 2, K111N (Table 1) [14]. MDA-MB-435S, MDA-MB-468, and MDA-MB-231 cells were maintained in Dulbecco's Modified Eagle's Medium (Cellgro; Mediatech, Inc., Herndon, CA) with 10% fetal bovine serum (FBS) (Gemini Bio-Products, Inc., Woodland, CA), 100 U/ml penicillin, 100 U/ml streptomycin, and 2 mM glutamine. The remaining cell lines were maintained in RPMI-1640 medium (Cellgro; Mediatech, Inc.) supplemented with 10% FBS, 100 U/ml penicillin, 100 U/ml streptomycin, and 2 mM glutamine. All cells were grown at 37°C in a humidified atmosphere with 5% CO_2 and were in logarithmic growth phase at initiation of the experiments.

Table 1. Genotype of *PIK3CA* in *HER2*-amplified breast cancer cell lines

Cell line	Genotype of *PIK3CA*
BT474	K111N
ZR75-30	wt
SKBR-3	wt
HCC1419	wt
MDA-MB-361	E545K
MDA-MB-453	H1047R
HCC1954	H1047R
UACC893	H1047R

wt, wild-type.

drugs

Trastuzumab was obtained from the Kobe University Hospital pharmacy. CL-387,785, a dual inhibitor of EGFR and HER2 [25], and LY294002, a PI3K inhibitor, were purchased from Calbiochem (San Diego, CA). Stock solutions were prepared in dimethyl sulfoxide (DMSO) and stored at −20°C. Before each experiment, drugs were diluted in fresh media. The final DMSO concentration was <0.1% for all experiments.

antibodies and western blotting

Cells were washed with ice-cold phosphate-buffered saline and scraped immediately after adding lysis buffer [20 mM Tris (pH 7.5), 150 mM NaCl, 10% glycerol, 1% Nonidet P-40, and 2 mM EDTA] containing protease and phosphatase inhibitors (100 mM NaF, 1 mM phenylmethylsulfonyl fluoride, 1 mM Na_3VO_4, 2 μg/ml aprotinin, and 5 μg/ml leupeptin). Lysates were centrifuged at 14 000 relative centrifugal force for 10 min. Supernatants were collected as protein extract and then separated by electrophoresis on 7.6% polyacrylamide–sodium dodecyl sulfate gels, followed by transfer to nitrocellulose membranes (Millipore Corporate Headquarters, Billerica, MA) and detection by immunoblotting using an enhanced chemiluminescence system (New England Nuclear Life Science Products, Inc., Boston, MA). The resulting signals were digitally quantified using the ImageJ software (www.nih.gov). Phospho-HER2/ErbB2 (Thr1221/1222), phospho-p70 S6 Kinase (Thr389), phospho-Akt (Ser473)(D9E), and PathScan(R) Multiplex Western Cocktail I were purchased from Cell Signaling Technology (Beverly, MA). The phospho-1/2 (pT185/pY187) antibody was purchased from Biosource International Inc. (Camarillo, CA), the c-erbb-2 antibody from Chemicon (Billerica, MA), and β-actin antibody from Sigma-Aldrich (St Louis, MO).

cell growth assay

Growth inhibition was assessed using the 3-(4,5-dimethylthiazol-2-yl)-5-(3-carboxymethoxyphenyl)-2-(4-sulfophenyl)-2H-tetrazolium (MTS) assay (Promega, Madison, WI), a colorimetric method for determining the number of viable cells based on the bioreduction of MTS to a soluble formazan product, which is detectable by spectrophotometry at a wavelength of 490 nm. Cells were diluted in 160 μl/well of maintenance cell culture media and plated in 96-well flat-bottom plates (Corning, Inc., Corning, NY). After a 96-h growth period, the number of cells required to obtain an absorbance of 1.3–2.2, the linear range of the assay, was

determined for each cell line beforehand. The number of cells per well used in the subsequent experiments were as follows: MCF-7, 2000; MDA-MB-361, 8000; HCC1954, 2500; MDA-MB-453, 7000; UACC893, 7500; CAMA-1, 6000; MDA-MB-435S, 2000; ZR75-30, 7500; HCC70, 4000; HCC1419, 8000; BT474, 3000; SKBR-3, 2500; BT549, 2000; T47D, 2500; ZR75-1, 7500; MDA-MB-415, 5000; and MDA-MB-231, 2500. At 24 h after plating, cell culture media were replaced with 10% FBS-containing media with and without trastuzumab or CL-387,785, followed by incubation for an additional 120 h. Trastuzumab and CL-387,785 concentrations ranged from 33 ng/ml to 100 μg/ml and from 3.3 nM to 10 μM, respectively. A total of 6–12 plate wells were set for each experimental point, and all experiments were carried out at least in triplicate. Data are expressed as percentage of growth relative to that of untreated control cells.

generation of *in vitro* BT474-TR

To generate a cell line resistant to trastuzumab, BT474 cells were continuously exposed to 100 μg/ml trastuzumab. To confirm the emergence of resistant clones, MTS assays were carried out every five passages after allowing cells to grow in drug-free conditions for at least 4 days. After 11 months of drug exposure, cells showed sufficient resistance (Figure 1) and were designated as BT474-TR. For controls, BT474 parental cells were concomitantly maintained without trastuzumab, and drug sensitivity was compared with trastuzumab-conditioned cells. No significant change in the sensitivity to trastuzumab was observed in parental cells during the drug-exposure period (data not shown).

results

inhibitory effect of trastuzumab on growth in breast cancer cell lines

We first screened 17 breast cancer cell lines for *in vitro* growth inhibition using trastuzumab. We confirmed that all relatively sensitive cell lines were *HER2*-amplified (Figure 2A). Among eight *HER2*-amplified cell lines, those with hotspot mutations in *PIK3CA* appeared resistant compared with the remaining cell lines (Figure 2B and C). We categorized BT474 as a *PIK3CA*-wild-type cell line in this study, based on reports showing that the K111N mutation lack ability of transformation and its influence on downstream signaling is negligible [18, 26]. A significant difference in sensitivity at 10 μg/ml trastuzumab was observed between *PIK3CA*-wild-type and -mutant cells (Figure 2C; $P = 0.010$). Protein expression levels of p110-α, the product of *PIK3CA*, were not correlated with sensitivity to trastuzumab (Figure 2C).

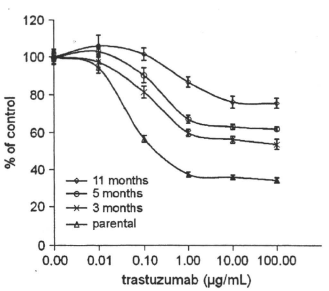

Figure 1. Development of BT474-TR. BT474 cells were continuously exposed to 100 μg/ml trastuzumab. BT-474 and trastuzumab-conditioned BT474 cells were grown in 10% serum-containing media for 5 days in the presence of various concentrations of trastuzumab. The percentage of viable cells is shown relative to that of the untreated control and plotted on the *y*-axis, whereas trastuzumab concentrations are plotted on the *x*-axis. Each data point represents the mean value and standard deviation of 6–12 replicate wells. Trastuzumab resistance increased in cells in a time-dependent manner. After 11 months, cells were designated as BT474-TR.

association between *PIK3CA* mutations and HER2-TKI resistance

Lapatinib, a HER2-TKI which may potentially overcome trastuzumab resistance, has been used in clinical settings [21]. We therefore tested a commercially available HER2-TKI, CL-387,785 [25], on *HER2*-amplified breast cancer cells. As shown in Figure 2D, cell lines with hotspot *PIK3CA* mutations showed resistance to CL-387,785. A statistically significant difference in sensitivity to 1 μM CL-387,785 was observed between *PIK3CA*-wild-type and -mutant cells (Figure 2C; $P = 0.001$) [24].

We then established a trastuzumab-resistant BT474 cell line (BT474-TR), a model of secondary resistant cells, by continuous exposure to trastuzumab (see 'Materials and methods' section). In contrast to *PIK3CA*-mutant cells, which showed primary resistance to trastuzumab, BT474-TR cells remained sensitive to CL-387,785 (Figure 3), which indicates that secondary resistant cells maintain dependency on HER2 signaling for growth.

association between phosphorylation change in S6K and growth inhibition by HER2-targeted agents

To identify potential pharmacodynamic markers of sensitivity to HER2-targeted therapy, we examined changes in phosphorylation of HER2 and representative downstream signaling molecules in 10% FBS-containing media with or without 10 μg/ml trastuzumab or 1 μM CL-387,785 (Figure 4A). The trastuzumab concentration was selected based on maintained growth inhibition (Figure 2B) and wide use in previous studies [11, 19]. The 1-μM CL-387,785 concentration was selected based on the approximate maximum plasma concentration of most TKIs available in clinics to date, including lapatinib [27], and use in previous studies [28, 29].

Trastuzumab treatment resulted in moderate phosphorylation inhibition of Akt and/or S6K in cell lines with wild-type *PIK3CA*. In contrast, no significant changes in Akt and S6K phosphorylation were observed in cell lines with hotspot mutant *PIK3CA*, as well as in BT474-TR cells. Although in ZR75-30, trastuzumab treatment appeared to inhibit phospho-ERK1/2, no significant changes were observed in other sensitive cells, namely BT474 and SKBR-3 (Figure 4A). In addition, phospho-ERK1/2 levels increased in MDA-MB-361 and UACC893, which indicates the presence of compensational cell signaling. Further, with the exception of HCC1419, treatment with CL-387,785 resulted in significant inhibition of Akt and S6K phosphorylation in BT474-TR and *PIK3CA*-wild-type cells, whereas residual phosphorylation signals were observed in all *PIK3CA* hotspot mutant cells.

doi:10.1093/annonc/mdp304 | 257

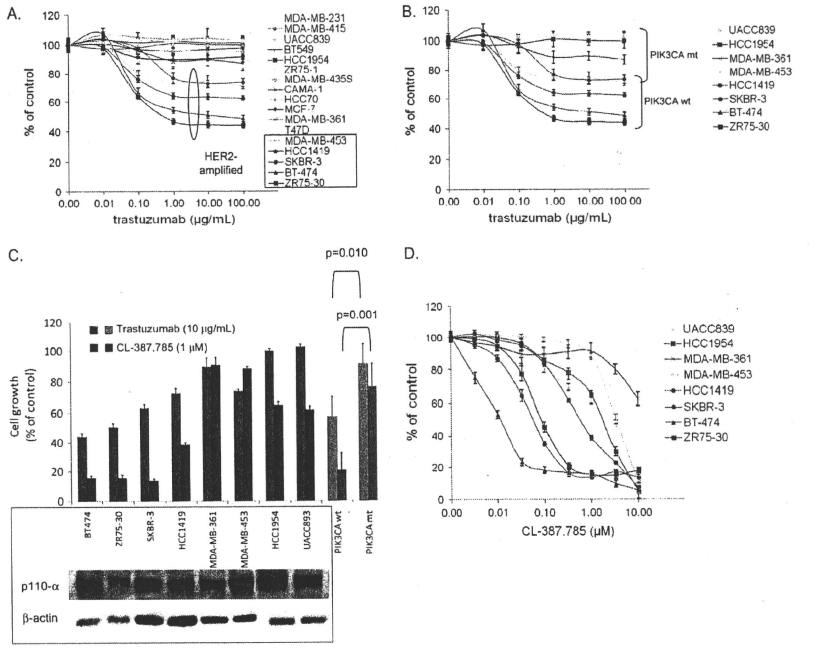

Figure 2. Effect of trastuzumab and CL-387,785 on growth inhibition in breast cancer cells *in vitro* [(**A**) trastuzumab on 17 breast cancer cell lines; (**B**) and (**D**) trastuzumab and CL-387,785 on eight *HER2*-amplified cell lines, respectively]. Breast cancer cells were grown in 10% serum-containing media for 5 days in the presence of various concentrations of trastuzumab (**A** and **B**) or CL-387,785 (**D**). The percentage of viable cells is shown relative to that of the untreated control and plotted on the *y*-axis, whereas trastuzumab and CL-387,785 concentrations are plotted on the *x*-axis. Each data point represents the mean value and standard deviation of 6–12 replicate wells. (**C**, top) Mean percentage of control and standard deviation of 6–12 replicate wells treated with 10 μg/ml trastuzumab and 1 μM CL-387,785, as well as those of *PIK3CA*-wild-type and -mutant cell lines (bottom), were plotted. (**C**, bottom) Protein expression of p110-α in *HER2*-amplified breast cancer cells. Blots were stripped and re-probed for β-actin as loading control.

Phosphorylation signals were then quantified and correlated with growth inhibition caused by trastuzumab and CL-387,785. As shown in Figure 4B, the closest association was observed between phospho-S6K changes and growth inhibition caused by trastuzumab and CL-387,785 [correlation coefficient (r), 0.811]. Further, close associations between phospho-S6K and cell growth were consistent when analyzed for trastuzumab and CL-387,785 separately (r for phospho-S6K versus growth: 0.8487 and 0.6970 for trastuzumab and CL-387,785, respectively).

dependency of *HER2*-amplified breast cancer cells on PI3K pathway

Given that inhibition of the PI3K pathway is critical in distinguishing cells sensitive from resistant to HER2-targeted agents (Figure 4B), we evaluated cell lines for the effects of LY294002, a PI3K inhibitor. As shown in Figure 5A, with the exception of ZR75-30, LY294002 induced a >30% growth inhibition compared with control in all cell lines. No significant difference in LY294002 sensitivity was observed between *PIK3CA*-mutant and -wild-type cell lines (Figure 5; $P = 0.655$). These results indicate that most *HER2*-amplified cells at least partly depend on the PI3K pathway regardless of the presence or absence of *PIK3CA* hotspot mutations.

To further gain insight into this concept, we evaluated phosphorylation levels of Akt and ERK1/2 in protein extracts obtained from cells under serum-starved conditions for 24 h. As shown in Figure 5B, despite the absence of serum factors, all *HER2*-amplified breast cancer cells showed a high level of phospho-Akt, regardless of *PIK3CA* genotype. High levels of phospho-Akt were also observed in MDA-MB-468, which lacks PTEN [30], and T47D, which harbors a *PIK3CA* mutation

(H1047R) [14]. These two cell lines do not show *HER2* amplification [23]. In contrast, no significant levels of phospho-Akt were observed in MDA-MB-231 and MDA-MB-435S, which show no *HER2* amplification, *PIK3CA* mutation, or PTEN loss [14, 23]. Further, with the exception of MDA-MB-231, all cell lines showed very low levels of phospho-ERK1/2 under serum-starved conditions. MDA-MB-231, in particular, was reported to contain double activating mutations in KRAS (G13D) and BRAF (G464V), whereas MDA-MB-435S showed an activating mutation in BRAF alone (V600E) [31]. These findings further support the concept that *HER2*-amplified cells tend to have HER2-PI3K signaling axis and they are thus dependent on the PI3K pathway rather than on extracellular signal-regulated kinase pathway.

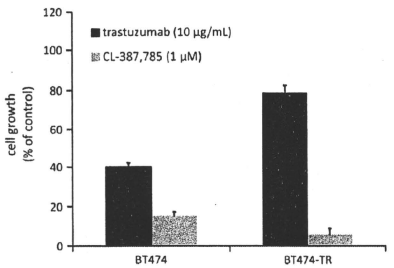

Figure 3. Effect of trastuzumab and CL-387,785 on growth inhibition in BT-474 and BT474-TR cells. Mean percentage of control and standard deviation of 6–12 replicate wells treated with 10 μg/ml trastuzumab and 1 μM CL-387,785 were plotted. BT474-TR remains sensitive to CL-387,785.

discussion

In this study, we show that gain-of-function mutations in *PIK3CA* genes are associated with trastuzumab resistance in naturally derived breast cancer cell lines showing *HER2* amplification. This finding is consistent with a recent study by Berns et al. [19] reporting trastuzumab resistance in SKBR-3 cells transfected with mutant *PIK3CA* (H1047R) compared with GFP control. Transfection of wild-type *PIK3CA*, however, appeared to equally cause trastuzumab resistance [19]. This observation does not identify either quantitative or qualitative changes in *PIK3CA* mutation as the major factor in developing trastuzumab resistance. In the present study, no clear association was observed between *PIK3CA* protein (p110-α) expression levels and *in vitro* sensitivity to trastuzumab

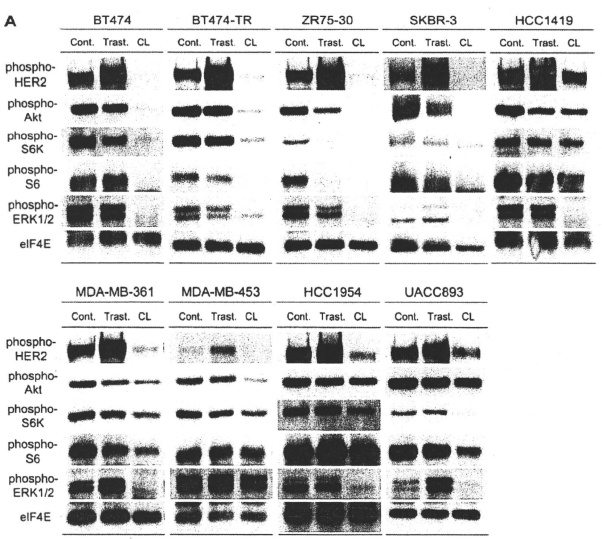

Figure 4. (A) Expression of phosphorylated-HER2, -Akt, -S6K, -S6 and -ERK1/2 in HER2-amplified breast cell lines with and without treatment with trastuzumab (10 μg/ml) and CL-387,785 (1 μM). Breast cell lines grown in 10% serum-containing media were lysed and immunoblotted for each protein. Blots were stripped and re-probed for eIF4E as loading control.

doi:10.1093/annonc/mdp304

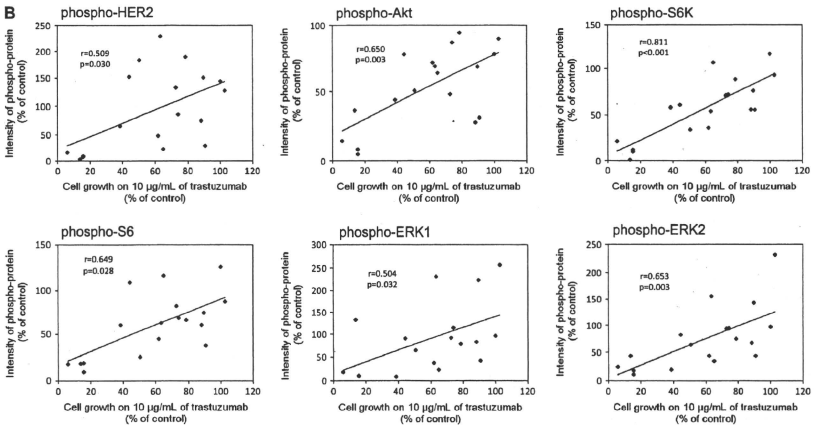

Figure 4. (Continued) (B) Correlation between changes in phosphorylation of HER2 signaling molecules and cell growth. Immunoblot quantification was carried out by densitometry using ImageJ software. Correlations were analyzed by calculating Pearson's correlation coefficient.

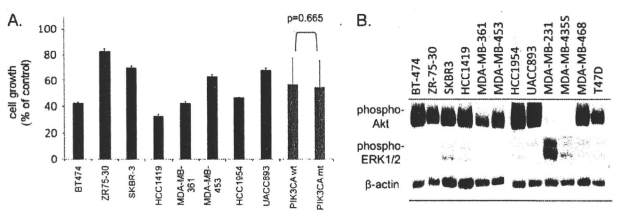

Figure 5. (A) Effect of LY294002 on growth inhibition in HER2-amplified breast cancer cell lines. Mean percentage of control and standard deviation of 6–12 replicate wells treated with 10 μM LY294002 were plotted. (B) Protein expression of phospho-Akt and phospho-ERK1/2 in HER2-amplified breast cancer cells under serum-starved condition. Blots were stripped and re-probed for β-actin as loading control.

(Figure 2C). A study by Haverty et al. [32], which analyzed copy number alterations in 51 breast tumors using a high-resolution single nucleotide polymorphism array, showed no gain in copy number on chromosome 3p, the location of the *PIK3CA* gene. These results indicate that qualitative changes in the *PIK3CA* gene itself may cause trastuzumab resistance in naturally derived breast cancer cells.

The CL-387,785 HER2-TKI was first evaluated to identify groups of compounds which may overcome trastuzumab resistance. Of note, results show an association between *PIK3CA* hotspot mutations and CL-387,785 resistance. Further, the difference in sensitivity between *PIK3CA*-wild-type and -mutant cell lines was more significant for CL-387,785 than for trastuzumab (Figure 2C). These results are consistent with a recent study by Eichhorn et al. [22], which showed that transfection of mutant *PIK3CA* (H1047R) in BT474 cells, which are sensitive to lapatinib, results in drug resistance. In contrast, the results of the present study show that BT474-TR cells remain highly sensitive to CL-387,785, which is consistent with a previous study by Konecny et al. [20] which reported that lapatinib remains active against cell lines selected by long-term exposure to trastuzumab. Although the study did not show the effect of lapatinib on cell signaling in secondary resistant cells, our present findings indicate that BT474-TR remains dependent on HER2/PI3K signaling and sensitive to HER2-TKI (Figure 4A).

We then evaluated LY294002 as a model PI3K inhibitor. Results show that *HER2*-amplified cells are generally sensitive to LY294002 regardless of *PIK3CA* genotype (Figure 5A), which indicates that *HER2* amplification is associated with dependency on PI3K pathway. Supporting this notion, all *HER2*-amplified breast cancer cells have high level of phosphorylation of Akt even in serum-starved condition. The Akt phosphorylation levels observed in *HER2*-amplified cells

were equivalent to those in MDA-MB-468 and T47D cells, which were reported to contain PTEN loss and a *PIK3CA* hotspot mutation without *HER2* amplification, respectively [23]. These findings therefore indicated that *HER2* amplification itself may have equivalent biological effect on PI3K signaling with PTEN loss or *PIK3CA* hotspot mutation. In addition, our results are consistent with a recent study by Oda et al. [33], in which they showed that HER2 and/or HER3 overexpression, PTEN, or *PIK3CA* mutations occur almost exclusively in breast and other cancer cell lines.

Findings in past and present studies may potentially lead to beneficial clinical applications. For *HER2*-amplified breast cancer showing no *PIK3CA* mutations, trastuzumab is likely to be effective, with possible rescue using HER2-TKIs in cases of relapse. For *HER2*-amplified breast cancer with *PIK3CA* mutations, inhibitors against molecules of the PI3K pathway are possibly more effective than anti-HER2 agents, which are unlikely to be beneficial.

In addition to pharmacogenetic approaches, including *PIK3CA* genotyping, pharmacodynamic markers are potentially powerful tools in individualized use of molecularly targeted therapy. In a number of previous pharmacodynamic studies on HER2- or EGFR-targeted therapy, phospho-Akt was used as a surrogate marker for PI3K pathway activity [34, 35]. In the present study, however, growth inhibition is more closely associated with changes in phospho-S6K than that in phospho-Akt. These findings indicate that the prediction of tumor response to trastuzumab may strongly benefit from measurements of S6K phosphorylation levels. The cause of the discrepancy between the association of cell growth with phospho-Akt and that with phospho-S6K, however, remains unclear. It may be due to the difference in sensitivity of phospho-specific antibodies used in the present study or the higher sensitivity of phospho-Akt to positive feedback signals following initial inhibition of the PI3K pathway compared with phospho-S6K.

The present study shows several limitations. First, although a relatively large panel of *HER2*-amplified breast cancer cell lines ($N = 8$) were used, the properties of all HER2-overexpressing breast tumors are not necessarily represented. Despite HER2 amplification being retained, particular tumor subtypes may have been selected in the establishment of cell lines. Secondly, in addition to inhibition of HER2 signaling, a few studies have indicated the contribution of antigen-dependent cellular cytotoxicity (ADCC) in the antitumor effect of trastuzumab. Because ADCC only works in *in vivo* conditions, our current data do not necessarily deny the potential effect of trastuzumab on tumors showing *PIK3CA* mutations [36]. Thirdly, although wild-type *PIK3CA* appeared necessary for trastuzumab sensitivity *in vitro*, other factors may be involved, as shown by results showing moderate resistance of HCC1419 to trastuzumab (Figure 2C). The mechanisms of *PIK3CA*-unrelated resistance remain unknown but are under current investigation in our laboratory.

In conclusion, our findings show an association between the presence of *PIK3CA* hotspot mutations and resistance to not only trastuzumab but also HER2-TKI in naturally derived *HER2*-amplified breast cancer cell lines. Further, PI3K inhibitors are potentially effective in overcoming trastuzumab resistance caused by *PIK3CA* mutations. Assessment of S6K phosphorylation levels may be a useful pharmacodynamic marker correlated to the antitumor effect of HER2-targeted therapy. A better understanding of these findings, however, may require further investigation in clinical trials and concomitant translational studies.

funding

Grant-in-Aid for Young Scientists (B) from Ministry of Education, Culture, Sports, Science and Technology of Japan to T.M.; AstraZeneca Research Grant 2007 to T.M.; Kobe University Medical School Research Grant for Young Scientists to T.M.; Grants-in-Aid for Cancer Research from Ministry of Health, Labor and Welfare of Japan to H.M.

references

1. McPherson K, Steel CM, Dixon JM. ABC of breast diseases. Breast cancer-epidemiology, risk factors, and genetics. BMJ 2000; 321: 624–628.
2. Parkin DM, Bray F, Ferlay J, Pisani P. Global cancer statistics, 2002. CA Cancer J Clin 2005; 55: 74–108.
3. Slamon DJ, Godolphin W, Jones LA et al. Studies of the HER-2/neu proto-oncogene in human breast and ovarian cancer. Science 1989; 244: 707–712.
4. Slamon DJ, Clark GM, Wong SG et al. Human breast cancer: correlation of relapse and survival with amplification of the HER-2/neu oncogene. Science 1987; 235: 177–182.
5. Slamon DJ, Leyland-Jones B, Shak S et al. Use of chemotherapy plus a monoclonal antibody against HER2 for metastatic breast cancer that overexpresses HER2. N Engl J Med 2001; 344: 783–792.
6. Piccart-Gebhart MJ, Procter M, Leyland-Jones B et al. Trastuzumab after adjuvant chemotherapy in HER2-positive breast cancer. N Engl J Med 2005; 353: 1659–1672.
7. Romond EH, Perez EA, Bryant J et al. Trastuzumab plus adjuvant chemotherapy for operable HER2-positive breast cancer. N Engl J Med 2005; 353: 1673–1684.
8. Buzdar AU, Ibrahim NK, Francis D et al. Significantly higher pathologic complete remission rate after neoadjuvant therapy with trastuzumab, paclitaxel, and epirubicin chemotherapy: results of a randomized trial in human epidermal growth factor receptor 2-positive operable breast cancer. J Clin Oncol 2005; 23: 3676–3685.
9. Vogel CL, Cobleigh MA, Tripathy D et al. Efficacy and safety of trastuzumab as a single agent in first-line treatment of HER2-overexpressing metastatic breast cancer. J Clin Oncol 2002; 20: 719–726.
10. Scaltriti M, Rojo F, Ocana A et al. Expression of p95HER2, a truncated form of the HER2 receptor, and response to anti-HER2 therapies in breast cancer. J Natl Cancer Inst 2007; 99: 628–638.
11. Xia W, Liu LH, Ho P, Spector NL. Truncated ErbB2 receptor (p95ErbB2) is regulated by heregulin through heterodimer formation with ErbB3 yet remains sensitive to the dual EGFR/ErbB2 kinase inhibitor GW572016. Oncogene 2004; 23: 646–653.
12. Nagata Y, Lan KH, Zhou X et al. PTEN activation contributes to tumor inhibition by trastuzumab, and loss of PTEN predicts trastuzumab resistance in patients. Cancer Cell 2004; 6: 117–127.
13. Samuels Y, Wang Z, Bardelli A et al. High frequency of mutations of the PIK3CA gene in human cancers. Science 2004; 304: 554.
14. Saal LH, Holm K, Maurer M et al. PIK3CA mutations correlate with hormone receptors, node metastasis, and ERBB2, and are mutually exclusive with PTEN loss in human breast carcinoma. Cancer Res 2005; 65: 2554–2559.
15. Campbell IG, Russell SE, Choong DY et al. Mutation of the PIK3CA gene in ovarian and breast cancer. Cancer Res 2004; 64: 7678–7681.
16. Lee JW, Soung YH, Kim SY et al. PIK3CA gene is frequently mutated in breast carcinomas and hepatocellular carcinomas. Oncogene 2005; 24: 1477–1480.
17. Isakoff SJ, Engelman JA, Irie HY et al. Breast cancer-associated PIK3CA mutations are oncogenic in mammary epithelial cells. Cancer Res 2005; 65: 10992–11000.

doi:10.1093/annonc/mdp304

18. Gymnopoulos M, Elsliger MA, Vogt PK. Rare cancer-specific mutations in PIK3CA show gain of function. Proc Natl Acad Sci U S A 2007; 104: 5569–5574.
19. Berns K, Horlings HM, Hennessy BT et al. A functional genetic approach identifies the PI3K pathway as a major determinant of trastuzumab resistance in breast cancer. Cancer Cell 2007; 12: 395–402.
20. Konecny GE, Pegram MD, Venkatesan N et al. Activity of the dual kinase inhibitor lapatinib (GW572016) against HER-2-overexpressing and trastuzumab-treated breast cancer cells. Cancer Res 2006; 66: 1630–1639.
21. Cameron D, Casey M, Press M et al. A phase III randomized comparison of lapatinib plus capecitabine versus capecitabine alone in women with advanced breast cancer that has progressed on trastuzumab: updated efficacy and biomarker analyses. Breast Cancer Res Treat 2008; 112: 533–543.
22. Eichhorn PJ, Gili M, Scaltriti M et al. Phosphatidylinositol 3-kinase hyperactivation results in lapatinib resistance that is reversed by the mTOR/phosphatidylinositol 3-kinase inhibitor NVP-BEZ235. Cancer Res 2008; 68: 9221–9230.
23. Lacroix M, Leclercq G. Relevance of breast cancer cell lines as models for breast tumours: an update. Breast Cancer Res Treat 2004; 83: 249–289.
24. Mukohara T, Shimada H, Ogasawara N et al. Sensitivity of breast cancer cell lines to the novel insulin-like growth factor-1 receptor (IGF-1R) inhibitor NVP-AEW541 is dependent on the level of IRS-1 expression. Cancer Lett 2009; 282: 14–24.
25. Discafani CM, Carroll ML, Floyd MB Jr et al. Irreversible inhibition of epidermal growth factor receptor tyrosine kinase with in vivo activity by N-[4-[(3-bromophenyl)amino]-6-quinazolinyl]-2-butynamide (CL-387,785). Biochem Pharmacol 1999; 57: 917–925.
26. Zhang H, Liu G, Dziubinski M et al. Comprehensive analysis of oncogenic effects of PIK3CA mutations in human mammary epithelial cells. Breast Cancer Res Treat 2008; 112: 217–227.
27. Burris HA III, Hurwitz HI, Dees EC et al. Phase I safety, pharmacokinetics, and clinical activity study of lapatinib (GW572016), a reversible dual inhibitor of epidermal growth factor receptor tyrosine kinases, in heavily pretreated patients with metastatic carcinomas. J Clin Oncol 2005; 23: 5305–5313.
28. Shimamura T, Li D, Ji H et al. Hsp90 inhibition suppresses mutant EGFR-T790M signaling and overcomes kinase inhibitor resistance. Cancer Res 2008; 68: 5827–5838.
29. Koivunen JP, Mermel C, Zejnullahu K et al. EML4-ALK fusion gene and efficacy of an ALK kinase inhibitor in lung cancer. Clin Cancer Res 2008; 14: 4275–4283.
30. Stemke-Hale K, Gonzalez-Angulo AM, Lluch A et al. An integrative genomic and proteomic analysis of PIK3CA, PTEN, and AKT mutations in breast cancer. Cancer Res 2008; 68: 6084–6091.
31. Hollestelle A, Elstrodt F, Nagel JH et al. Phosphatidylinositol-3-OH kinase or RAS pathway mutations in human breast cancer cell lines. Mol Cancer Res 2007; 5: 195–201.
32. Haverty PM, Fridlyand J, Li L et al. High-resolution genomic and expression analyses of copy number alterations in breast tumors. Genes Chromosomes Cancer 2008; 47: 530–542.
33. Oda K, Okada J, Timmerman L et al. PIK3CA cooperates with other phosphatidylinositol 3′-kinase pathway mutations to effect oncogenic transformation. Cancer Res 2008; 68: 8127–8136.
34. Baselga J, Albanell J, Ruiz A et al. Phase II and tumor pharmacodynamic study of gefitinib in patients with advanced breast cancer. J Clin Oncol 2005; 23: 5323–5333.
35. Mohsin SK, Weiss HL, Gutierrez MC et al. Neoadjuvant trastuzumab induces apoptosis in primary breast cancers. J Clin Oncol 2005; 23: 2460–2468.
36. Clynes RA, Towers TL, Presta LG, Ravetch JV. Inhibitory Fc receptors modulate in vivo cytotoxicity against tumor targets. Nat Med 2000; 6: 443–446.